Prime Editing Efficiency and Fidelity are Enhanced in the Absence of Mismatch Repair

Ferreira da Silva J[1,2#], Oliveira GP[1#], Arasa-Verge EA[1], Moretton A[1,2], Timelthaler G[1], Jiricny J[4,5], Loizou JI[1,2*]

[1]Institute of Cancer Research, Department of Medicine I, Comprehensive Cancer Centre, Medical University of Vienna, Borschkegasse 8a, 1090 Vienna, Austria
[2]CeMM Research Center for Molecular Medicine of the Austrian Academy of Sciences, Vienna, Austria
[3]Institute of Life Sciences, University of Zurich, Winterthurerstrasse 190, 8057 Zurich, Switzerland
[4]Institute of Biochemistry of the ETH Zurich, Otto-Stern-Weg 3, 8093 Zurich, Switzerland.
[#]Equal contribution
*Correspondence

Correspondence: joanna.loizou@meduniwien.ac.at (JIL)

Running title

Enhancement of Prime Editing Efficiency and Fidelity by Ablation of Mismatch Repair

Keywords

Prime editing; mismatch repair; genome engineering; DNA repair

Abstract

Prime editing is a powerful genome engineering approach that enables the introduction of base substitutions, insertions and deletions, into any given genomic locus. But prime editing, at even the same locus, can exhibit wildly different efficiencies in various cell backgrounds. It is unclear what determines these variations in efficiencies in a given cellular context. Through a focused genetic screen targeting DNA repair factors, we show that the efficiency of prime editing is attenuated by the mismatch repair pathway. The accumulation of the mismatch repair protein MLH1 at sites of prime editing, indicates that mismatch repair acts at these regions to directly counteract the insertion of the edit. Consequently, ablation of mismatch repair yields an up to 17-fold increase in prime editing efficiency across different human cell lines, several types of edits and multiple genomic loci. Our results shed new light on the cellular

requirements for prime editing and identify that ablation of mismatch repair increases editing efficiency and fidelity.

Introduction

Genome editing technologies, using CRISPR-Cas, are powerful approaches that can be used for functional genomics, as well as for therapeutic applications (Jinek et al., 2012). Their optimal implementation, however, relies on a thorough understanding of the DNA metabolic pathways and mechanisms that are responsible for editing outcomes, as well as the activity of these pathways in different tissue contexts (Richardson et al., 2018; Yeh et al., 2019; Ferreira da Silva et al., 2021; Hussmann et al., 2021). Amongst the toolbox of Cas9 proteins that are used for genome engineering are Cas9 nucleases that can be directed to a specific region of the genome by a single-guide RNA (sgRNA). Following the generation of a DNA double-strand break (DSB), the endogenous cellular DNA end-joining pathways can repair the lesion in an error prone manner, leading to insertions and deletions (indels) that culminate in loss-of-function alleles (Bothmer et al., 2017). This approach can be further adapted to include a donor template, either single-stranded or double-stranded, containing a desired edit. Here, following the generation of a DNA DSB, homology directed repair (HDR) mediates the insertion of the desired template, thus editing the genome. This approach can be used to introduce or correct mutations with high precision. However, since HDR is an inefficient mechanism, depends on potentially deleterious DSBs and requires cell division, other approaches have been developed.

Amongst these are base editors (BE) which use nucleobase modification chemistry to efficiently and precisely incorporate single nucleotide variants into the genome of living cells (Komor et al., 2016; Gaudelli et al., 2017; Gu et al., 2021). BEs are however limited to single-base substitutions. Thus, more recently, prime editing (PE) was developed as a highly versatile genome editing approach that allows for targeted insertions, deletions and all possible combinations of base substitutions in a precise manner, independent on cell division (Anzalone et al., 2019). PE utilises a fusion of a Cas9(H840A) nickase (Jinek et al., 2012) and reverse transcriptase (RT) that is targeted to a precise genomic region by a PE guide RNA (pegRNA). The pegRNA encodes, in its 3’ extension region, the genetic information that is copied to the targeted genomic locus by the RT. The installation of the desired edit is dependent on the resolution of a DNA intermediate that contains redundant single-stranded DNA (ssDNA) flaps. Preferential 5’ flap excision and 3’ flap ligation drives the integration of the edit, resulting in a DNA heteroduplex containing one edited- and one non-edited strand (PE2). The editing outcome depends on the resolution of this heteroduplex. Utilising a sgRNA that directs the nicking of the non-edited strand, either concurrently to the edit installation

(PE3), or afterwards (PE3b), has been shown to increase PE efficiencies (Anzalone et al., 2019).

A notable feature of prime editing is its highly variable rates of efficiency across different genetic backgrounds, even within the same genomic region and using the same pegRNA (Anzalone et al., 2019). To address whether this could be explained by different DNA repair capacities, we performed a targeted genetic screen aimed at identifying DNA repair factors involved in PE. Here, we uncover an unexpected inhibitory role for the mismatch repair (MMR) pathway in PE and show that MMR localises to sites of PE to counteract edit installation. Thus, MMR depletion increases PE efficiency and fidelity across different edit sites, types and cell lines.

Results

A targeted genetic screen identifies the mismatch repair pathway as inhibitory for prime editing

To investigate the DNA repair requirements for PE, we conducted a targeted genetic screen, utilising a collection of isogenic knockout cell lines in the human near-haploid cell line HAP1 (**Supplementary Table 1**). The 32 targeted genes were selected to represent divergent functions within all known human DNA repair pathways. The library thus provided a comprehensive coverage of the DNA damage response. The cell lines received the PE machinery, including the Cas9(H840)-RT and a pegRNA encoding a 5-base pair (bp) deletion in the *HEK3* locus. Editing efficiency was then determined by amplicon sequencing of the genomic locus.

Wild-type HAP1 cells were remarkably inefficient at prime editing (<1% alleles edited). In contrast, isogenic HAP1 cell lines mutated at the *MLH*1, *PSM2*, *MSH2*, *EXO1* and *MSH3* loci displayed higher levels of PE (ranging from 2.3 to 7.9-fold) (**Figure 1A**). Deficiencies in other DNA repair pathways had little impact on the efficacy of prime editing. This finding clearly indicates that MMR plays an inhibitory role in PE. Of all MMR genes targeted in the screen, only the loss of *MSH6* failed to increase PE efficiency.

The MMR pathway evolved to correct base/base mispairs and indels arising in DNA during replication. Base/base mismatches and small indels of 1-3 nucleotides are recognised by the heterodimer MSH2-MSH6, whereas indels are generally recognised by the MSH2-MSH3 heterodimer (Drummond et al., 1995; Palombo et al., 1995, 1996; Acharya et al., 1996; Gradia et al., 1997). Detection of the lesion is followed by an ATP-dependent conformational change of these complexes and recruitment of the MLH1-PMS2 (Li and Modrich, 1995) or MLH1-

MLH3 (Lipkin et al., 2000) heterodimers. Assembly of this complex together with RFC and PCNA (Pluciennik et al., 2010) activates cryptic endonucleases of the PMS or MLH3 proteins, which then introduce DNA single-strand breaks (SSBs) into the nascent DNA strand in the vicinity of the mismatch. These SSBs act as entry points for EXO1, which degrades the nascent strand up to, and some distance past, the misincorporated nucleotide(s) (Kadyrov et al., 2006). The resulting gap is filled-in by polymerase δ and the remaining nick is ligated by DNA ligase I (Stojic et al., 2004; Iyer et al., 2006; Fishel, 2015). The edit introduced in our screen, a 5bp deletion, is a preferential target of the MSH2-MSH3 heterodimer, but not the MSH2-MSH6 heterodimer (Palombo et al., 1996), thus explaining the lack of an effect on editing upon loss of MSH6 (**Figure 1A**). This result highlights the highly specialised nature of the DNA damage response and shows that different edits might be addressed by distinct factors.

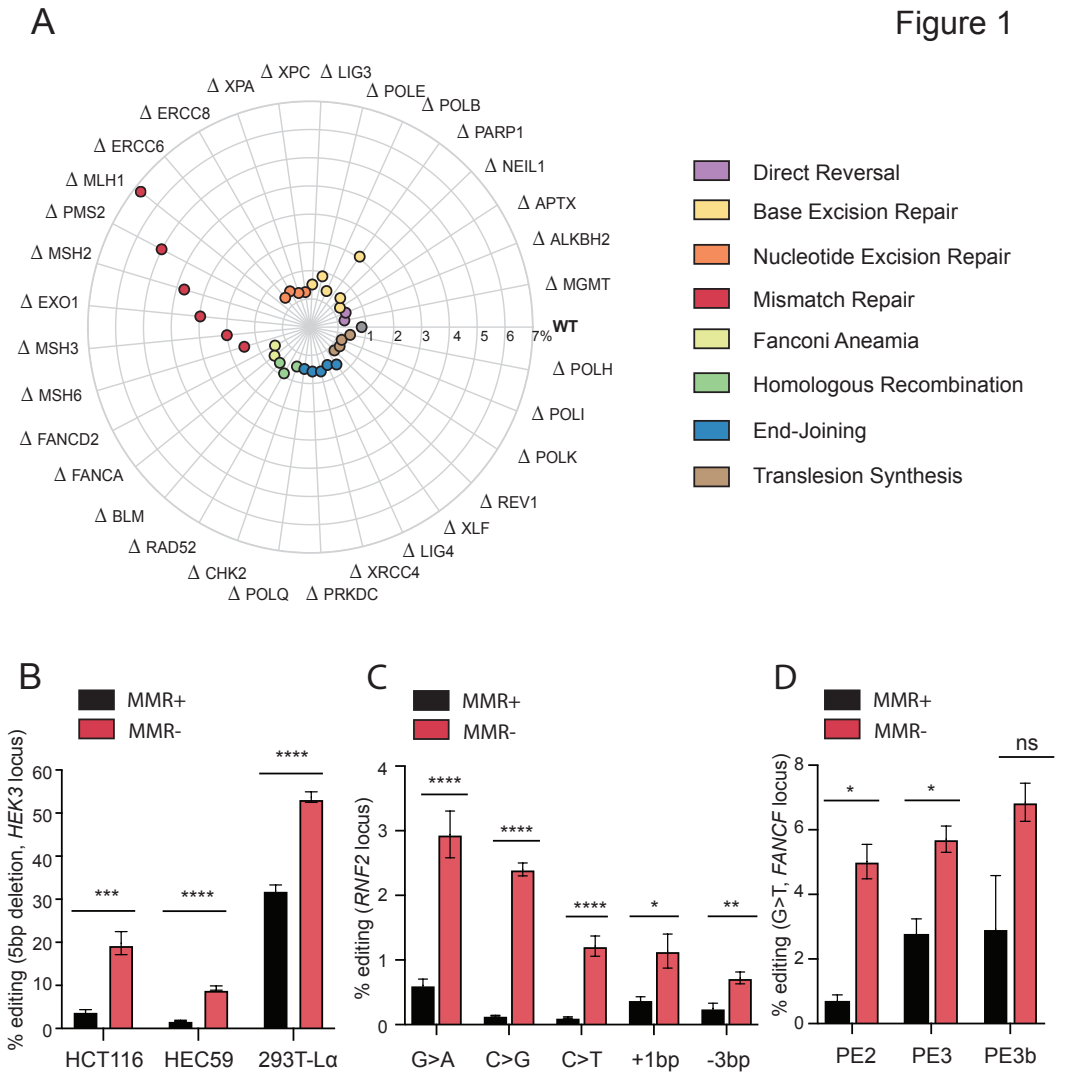

Figure 1: Mismatch repair inhibits prime editing in human cells. A) Genetic screen in a panel of 32 HAP1 isogenic knockout cell lines covering different DNA damage repair

pathways, as well as their wild-type (WT) counterpart, showing the efficiency of installation of a 5 base pair (bp) deletion in the *HEK3* locus, using PE2. Values correspond to editing efficiency, measured by amplicon sequencing analysis in two independent biological replicates, with two technical replicates each. Each radial line represents an increment of 1%. **B)** PE efficiency of a 5 bp deletion in the *HEK3* locus in different mismatch repair-deficient human cell lines, along with their respective complemented counterparts. Values correspond to editing efficiency, measured by amplicon sequencing analysis in three independent biological replicates, with two technical replicates each. **C)** PE efficiency of different types of edits (*RNF2* locus) in the HEC59 cell line complemented with chromosome 2 (MMR proficient; MMR+) and HEC59 cell line (MMR deficient; MMR-). Values correspond to editing efficiency, measured by amplicon sequencing analysis in three independent biological replicates, with two technical replicates each. **D)** Comparison of different types of PE efficiency (PE2, PE3 and PE3b) upon installation of a G>T substitution in the *FANCF* locus, in HEC59 cells complemented with chromosome 2 (MMR+) and HEC59 cells (MMR-). Values correspond to editing efficiency, measured by amplicon sequencing analysis in three independent biological replicates, with two technical replicates each. Ns, p-value non-significant; *, p-value < 0.05; **, p-value < 0.01; ***, p-value<0.001; ****, p-value < 0.0001.

Mismatch repair hinders PE2 and PE3 across several human cell lines, genomic loci and edits

To further explore the inhibitory role of MMR in PE, we measured editing efficiency and fidelity of the *HEK3* locus in a panel of MMR-deficient human cell lines, alongside their complemented counterparts. We used the colorectal cancer line HCT116, which is deficient for both MSH3 and MLH1, along with an HCT116 MMR-proficient cell line complemented with both chromosomes 5 and 3 (**Supplementary Figure 1A)** (Koi et al., 1994; Haugen et al., 2008). Additionally, the endometrial adenocarcinoma cell line HEC59, which is deficient for MSH2, was used together with its MMR-proficient counterpart that was complemented with chromosome 2 (**Supplementary Figure 1B**) (Umar et al., 1997). Finally, we used a doxycycline-inducible model of MLH1 deficiency in the embryonic kidney cell line HEK293T (293T-Lα) (**Supplementary Figure 1C**) (Cejka et al., 2003). All cell lines showed significantly increased PE2 editing (1.7 to 5-fold) when MMR was ablated, compared to their MMR-proficient counterparts (**Figure 1B**). Importantly, even though PE efficiencies were increased by MMR deficiency, this did not come at the expense of higher indel frequencies at the amplicon region (**Supplementary Figure 1D**). Indeed, we observed that loss of MMR prevented unwanted indels at the *HEK3* locus in the 293T-Lα cell line (**Supplementary Figure 1D**).

To investigate further the substrates of MMR in PE, we measured the editing efficiencies of a transition (G>A), two transversions (C>G and C>T), a 1 bp insertion and a 3 bp deletion, all within a different endogenous locus. We found that active MMR significantly diminished the efficiency of all these edits in HEC59 cells (ranging from 2.8 to 17-fold) (**Figure 1C**). To test

166 the inhibitory role of MMR on different types of PE, we measured the efficiency of PE2, PE3
167 and PE3b in the *FANCF* locus, via the installation of a G>T substitution. Editing efficiency was
168 improved by loss of MMR for all types of PE, albeit to a lesser extent for PE3b (**Figure 1D**). In
169 summary, MMR counteracts PE efficiency across different edits and different genomic loci.
170

171 **The mismatch repair factor MLH1 is directly recruited to sites of prime editing**

172 We hypothesized that MMR could reduce PE efficiency either directly at the edit site, or
173 indirectly by other mechanisms. To address this, we determined if the MMR factor MLH1 was
174 recruited to sites of active and ongoing editing, through co-localization with Cas9(H840)-RT.
175 Cas9(H840)-RT was directed to human repetitive telomeric regions, a strategy that has proven
176 efficient for CRISPR imaging (Chen et al., 2013) (**Figure 2A**). With this experimental
177 approach, Cas9(H840)-RT was shown to co-localise with TRF1, a major telomere-binding
178 protein (Wang et al., 2008) (**Supplementary Figures 2A-B**). Similarly, endogenous MLH1 co-
179 localised with Cas9(H840)-RT-foci, in a pegRNA-dependent manner (**Figures 2B-C**). Based
180 on these results, we postulate that PE inhibition by MMR occurs through recruitment of MMR
181 factors to sites of editing, where the heteroduplex DNA is recognised as a mismatch and
182 removed, using the non-edited strand as a template, and thus restoring the non-edited
183 sequence of nucleotides.

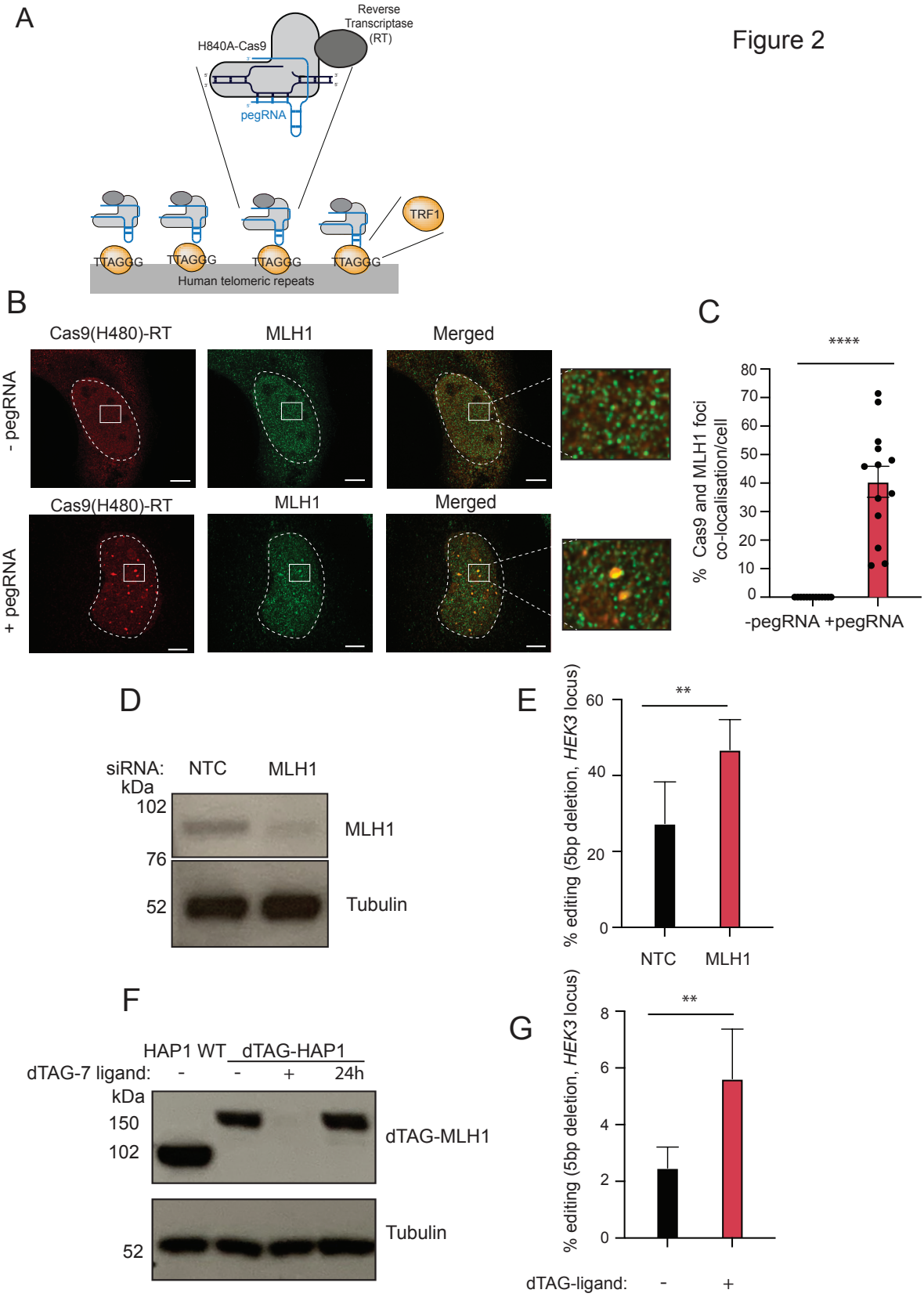

Figure 2: MLH1 is enriched at prime editing sites and its ablation can be exploited to increase prime editing efficiency. A) Schematic representation of the approach used to co-localise MLH1 at PE sites. The PE machinery is directed to human telomeric repetitive regions,

where the telomeric protein, TRF1, also binds. **B)** Representative super resolution images of Cas9(H490)-RT, MLH1 and both merged, in U2OS cells. Images were taken 24 hours following reverse transfection of Cas9(H480)-RT and in the presence or absence of a pegRNA targeting telomeric repeats. Scale bars = 5 µm **C)** Quantification of Cas9(H480)-RT foci that co-localise with MLH1. Values correspond to quantification of 13 cells in three independent biological replicates. **D)** Immunoblot for MLH1 and tubulin in HEK293 cell extracts three days post transfection with non-targeting and MLH1 siRNA pools (of four siRNAs). **E)** PE efficiency of a 5 bp deletion in the *HEK3* locus in HEK293 cells transfected with non-targeting and MLH1 siRNA pools, two days prior to PE vector delivery. Values correspond to editing efficiency, measured by Sanger sequencing and analysed by TIDE analysis (Brinkman et al., 2014), in three independent biological replicates, with two technical replicates each. **F)** Immunoblot for MLH1 and tubulin in HAP1 cell extracts. Expression of dTAG-MLH1 is abrogated upon 1-hour treatment with 500nM dTAG-7 ligand ('+' condition). Recovery of dTAG-MLH1 expression is visible 24 hours after ligand removal ('24h' condition) **G)** PE efficiency of a 5 bp deletion in the *HEK3* locus in HAP1 dTAG-MLH1 cells in the presence and absence of 500 nM dTAG-7. Values correspond to editing efficiency, measured by Sanger sequencing and analysed by TIDE analysis (Brinkman et al., 2014), in three independent biological replicates, with two technical replicates each. Ns, p-value non-significant; *, p-value < 0.05; **, p-value < 0.01; ****, p-value < 0.0001.

Mismatch repair inhibition can be exploited to increase prime editing efficiency

We next sought to inhibit MMR as a strategy to improve PE efficiency. Since MMR loss leads to increased mutational burden and genome instability (Jiricny, 2006), long-term inhibition of MMR is not desirable. Thus, to achieve transient MMR ablation, we depleted MLH1 in HEK293 cells with a pool of siRNAs (**Figure 2D**), and subsequently showed that this effectively increased PE efficiency in the *HEK3* locus (**Figure 2E**).

An alternative way to achieve transient loss of function is through targeted protein degradation. The degradation tag (dTAG) system has proved to be an efficient strategy for rapid and transient ligand-induced targeted protein degradation (Winter et al., 2015). Using CRISPR-mediated knock-in, we introduced the dTAG system into the *MLH1* locus of HAP1 cells which allowed for the targeted degradation of MLH1, after ligand treatment (**Figure 2F**). Upon MLH1 degradation, the efficiency of PE was increased by 2-fold (**Figure 2G**). Taken together, these results indicate that transient inhibition of MMR is a promising strategy to increase the efficiency of PE.

Discussion

Here, we describe an inhibitory role of the MMR pathway during PE, across different human cell lines, genomic loci and types of edits, thus challenging the current view that this is a pathway that is required for edit installation (Petri et al., 2021). We propose that MMR proteins recognise the heteroduplex DNA, containing the desired edit introduced by the pegRNA, as a mismatch. The mismatch is promptly removed, and the non-edited strand is used as a

232 template to restore the original sequence of nucleotides. Hence, suppression of MMR
233 increases PE efficiency.
234
235 Our findings suggest that the improvement in PE efficiencies upon loss of MMR activity does
236 not come at the cost of indel generation around the edit site, which would be an undesirable
237 outcome of editing. Much effort has gone into improving genome editing technologies through
238 both computational and experimental approaches aimed at improving editing efficiencies and
239 fidelity. While globally manipulating MMR in dividing cells would come at the expense of
240 mutations, precisely interfering with MMR at the edit site might offer an approach to specifically
241 perturb this pathway only at the sites of PE. Similar approaches have proved useful for
242 improving the efficiency of HDR (Charpentier et al., 2018; Rees et al., 2019), suggesting that
243 their development for PE might also be valuable.
244
245 The highly specialised nature of the DNA damage response suggests that different edits might
246 be dealt with by different pathways, and even different factors within the same pathway. Our
247 data on the lack of involvement of MSH6 in the repair of a 5bp deletion supports this
248 hypothesis. While it is known that MMR functions to repair base substitutions and small indels,
249 it remains to be seen what the size limitation of an edit is to be removed by this pathway, when
250 generated by PE. Future directions might provide a deeper understanding of the specificity
251 and size of MMR substrates in PE to determine if perturbing MMR could be used to enhance
252 the insertion of small tags such as histidine or hemagglutinin tags.
253
254 Overall, our data shed new light on the DNA repair mechanisms of a new and highly promising
255 genome editing technology. This knowledge can be applied in further development of prime
256 editors, as well as in the design of therapeutic strategies. Finally, taking into consideration the
257 expression levels of MMR factors in particular tissue or cell types might predict PE efficiencies.
258
259

260 Methods

261 Plasmids and oligos

262 DNA oligos were obtained from Integrated DNA Technologies (IDT) unless otherwise noted.
263 All plasmids used for prime editing experiments were obtained from Addgene (pCMV-PE2
264 no.132775, pU6-pegRNA-GG-acceptor no.132777). PegRNAs were cloned using BsaI
265 Golden Gate assembly (NEB), as described previously (Anzalone et al., 2019). The pegRNA
266 targeting telomeres included a stem loop extension as described in. SgRNAs utilized in PE3
267 and PE3b experiments were cloned in the plenti-sgRNA puro vector (Addgene no. 104990),

268 using BsmBI Golden Gate assembly (NEB), following the manufacturer's instructions. The
269 pegRNA targeting telomeres included a stem loop extension as described in (Chen et al.,
270 2013). Sequences of sgRNA and pegRNA constructs are listed in **Supplementary Table 2**.
271 All plasmids for mammalian cell experiments were purified using the Plasmid Plus Midi Kit
272 (Qiagen) or the Spin Miniprep Kit (Qiagen), both including endotoxin removal steps.
273
274 **Mammalian cell culture**
275 All cells were grown at 3% oxygen at 37°C and routinely checked for possible mycoplasma
276 contamination. Human HAP1 cells were obtained from Horizon Discovery and were grown in
277 Iscove's Modified Dulbecco's Medium (IMDM) (Gibco), containing L-glutamine and 25nM
278 HEPES and supplemented with 10% Fetal Bovine Serum (FBS) (Gibco) and 1%
279 Penincillin/Streptomycin (P/S) (Sigma-Aldrich). U2OS cells were purchased from ATCC cell
280 repository and cultured in DMEM (Gibco), supplemented with 10% FBS and 1% P/S. HEC59,
281 wild-type and complemented with chromosome 2, were provided by Josef Jiricny (ETH Zurich,
282 Switzerland) and cultured in F12 DMEM with 10% FBS and 1% P/S. HEC59 complemented
283 cells were cultured with 400 µg/mL of geneticin (G418, Gibco). HCT116 cells, wild-type and
284 complemented with both chromosomes 3 and 5, were provided by Josef Jiricny (ETH Zurich,
285 Switzerland) and cultured with McCoy's 5A medium (Gibco), with 10% FBS and 1% P/S.
286 HCT116 cells complemented with chromosomes 3 and 5 were cultured with 400 µg/mL
287 geneticin (G418, Gibco) and 6 ug/mL blasticidine (Invivogen). 293T-Lα were provided by Josef
288 Jiricny (ETH Zurich, Switzerland) and cultured in DMEM medium (Gibco) supplemented with
289 10% FBS or Tet-system approved FBS (Takara Bio), 1% P/S, 100 µg/mL zeocin (Gibco) and
290 300 µg/mL hygromycin (Gibco). 293T-Lα were grown in doxycycline (1µg/mL) for 7 days
291 before any experiment, to completely deplete MLH1 expression. Doxycycline was replenished
292 in the medium every 2 days.
293
294 **Focused DNA repair genetic screen**
295 CRISPR-Cas9 knockouts of DNA repair genes were generated in collaboration with Horizon
296 Genomics. Sequences of sgRNAs were designed by Horizon Genomics or with the use of
297 http://chopchop.cbu.uib.no/. sgRNA sequences and frameshift mutations can be found in
298 **Supplementary Table 1**.
299
300 For the genetic screen, 80,000 cells were seeded in technical duplicates in 12-well plates.
301 Cells were transfected the day after with 636ng of pCMV-PE2 and 159ng of the *HEK3* pegRNA
302 inducing a 5bp deletion, per well. 1.6uL Lipofectamine 2000 (ThermoFisher Scientific) were
303 used per well, following the manufacturer's instructions. A separate transfection control was
304 performed using 795ng of the pmaxGFP™ vector (Lonza). Medium containing transfection

305 reagents was removed 16h post-transfection. Transfection efficiency was measured 48h after
306 transfection, by determining the percentage of GFP+ cells by flow cytometry. Genomic DNA
307 was harvested 96h post-transfection, using the QUIAmp DNA Blood Mini kit (Quiagen),
308 following the manufacturer's instructions.
309
310 **Transfection and genomic DNA preparation of mismatch repair-deficient human cell**
311 **lines**
312 HEC59, HCT116 and HEK293Tα were seeded in 48-well plates in duplicates (50,000
313 cells/well). Transfections were performed the next day, using 1µL Lipofectamine 2000
314 (ThermoFisher Scientific) per well, following the manufacturer's instructions. Cells were
315 transfected with 320 ng of the pCMV-PE2 vector, 80 ng of the respective pegRNA and, for
316 PE3 and PE3b, 33.2 ng of the nicking sgRNA, per well. A transfection control was performed
317 in parallel, by transfecting 400 ng per well of the pmaxGFP^{TM} vector (Lonza).
318
319 Genomic DNA was extracted 96 hours after transfection, by removing the medium,
320 resuspending the cells in a lysis solution (100 µL DirectPCR Lysis Reagent (Cell) (Viagen
321 Biotech), 76 µL of water and 4 µL Proteinase K) and incubating 45 minutes at 55 ºC and 45
322 minutes at 85 ºC.
323
324 **High-throughput DNA sequencing of genomic samples**
325 Genomic sites of interest were amplified from genomic DNA samples and sequenced on an
326 Illumina Miseq or NextSeq, depending on the number of pooled samples. Amplification primers
327 containing Illumina forward and reverse primers **(Supplementary Table 2)** were used for a
328 first round of PCR (PCR1) to amplify the genomic region of interest. A mixture of staggered
329 forward primers was used to create complexity. PCR1 reactions were performed in a final
330 volume of 25 µL, using 0.5µM of each forward and reverse primers, 1 µL genomic DNA and
331 12.5 µL of Phusion U Multiplex PCR 2x Master Mix (ThermoFisher Scientific). PCR1 was
332 carried as following: 98 ºC 2 min, 30 cycles [98ºC 10 s, 61 ºC 20 s, 72 ºC 30 s], followed by a
333 final extension of 72 ºC for 7 min. Unique Illumina dual index barcode primer pairs were added
334 to each sample in a secondary PCR reaction (PCR2). PCR2 was performed in a final volume
335 of 25 µL, using 0.5 µM of each unique forward and reverse Illumina barcoding primer pair,1
336 µL of unpurified PCR1 reaction and 12.5 µL of of Phusion U Multiplex PCR 2x Master Mix.
337 PCR2 was carried as following: 98 ºC 2 min, 12 cycles [98ºC 10 s, 61 ºC 20 s, 72 ºC 30 s],
338 followed by a final extension of 72 ºC for 7 min. PCR products were analysed by
339 electrophoresis in a 1% (w/v) agarose gel and purified using magnetic AMPure XP beads
340 (Beckman Coulter), using a ratio of beads:PCR product of 2:1. DNA concentration was

341 measured by fluorometric quantification (Qubit, ThermoFisher Scientific) and sequenced on
342 an Illumina instrument, according to manufacturer's instructions.
343
344 Sequencing reads were demultiplexed using MiSeq Reporter (Illumina) and alignment of
345 amplicon sequences to a reference sequence was performed using CRISPResso 2 (Clement
346 et al., 2019). CRISPResso2 was ran in standard mode and prime editing yield was calculated
347 as: number of aligned reads containing the desired edit/total aligned reads. Percentage of
348 indels was calculated as: number of aligned reads containing indels that are not the desired
349 edit/ total number of aligned reads.
350
351 **siRNA transfections**
352 The following siRNAs from Dhamacon (used at a final concentration of 100nM) were used in
353 this study: MLH1 SMARTpool ON-TARGETplus (L-003906-00-0005) and Non-targeting
354 control SMARTpool ON-TARGETplus (D-001810-10-05). siRNA transfections in HEK293 cells
355 were performed using Dharmafect 1 following manufacturer´s instructions. siRNA delivery was
356 performed 48 hours prior to transfection of prime editing vectors.
357
358 **Generation of dTAG-MLH1 HAP1 cell line**
359 A targeting vector encoding for the BSD-dTAG sequence (amplified from pCRIS-PITChv2-
360 BSD-dTAG (BRD4) Addgene no.91792) surrounded by two 1kb-long homology arms
361 upstream and downstream of the start codon of MLH1 was generated using Gibson assembly
362 (NEB). An in-vitro transcribed sgRNA targeting the region spanning the start codon of MLH1
363 was generated as previously described (Richardson et al., 2018). Cas9 protein (IDT) together
364 with the targeting vector and in-vitro transcribed sgRNA were nucleofected into 200,000
365 haploid cells in 16-well strips, using a 4D Nucleofector (Lonza) and the program DS-118.
366 Three days after nucleofection, 10 µg/ml blasticidin (Invivogen) were added to the culture
367 medium for one week after which single and haploid clones were sorted into 96-well plates.
368 Clonal haploid populations were grown and validated for correct homology-directed repair by
369 LR-PCR and immuno blot analysis. dTAG-7 (R&D Systems), at the final concentration of 500
370 nM, was used to test target degradation in the generated clones and all further targeted protein
371 degradation experiments.
372
373
374 **Immunoblotting**
375 Cell extracts were prepared in RIPA lysis buffer (NEB) supplemented with protease inhibitors
376 (Sigma) and phosphatase inhibitors (Sigma, NEB). Immunoblots were performed using
377 standard procedures. Protein samples were separated by sodium dodecyl sulfate-

378 polyacrylamide gel electrophoresis (SDS-PAGE) (3–8% gradient gels, Invitrogen) and
379 subsequently transferred onto nitrocellulose membranes. Primary antibodies for MLH1
380 (554073, BD Pharmigen), MSH2 (ab52266, Abcam), MSH3 (ab69619, Abcam), Tubulin (3873,
381 Cell Signaling) and ß-Actin (A5060, Sigma) were used at 1:1,000. Secondary antibodies were
382 used at 1:5,000 (HRP-conjugated goat anti-mouse or anti-rabbit IgG from Jackson
383 Immunochemicals). Immunoblots were imaged using a Curix 60 (AGFA) table-top processor.
384
385 **Immunofluorescence**
386 U2OS cells were reverse transfected using PEI together with pCMV-PE2 in the presence and
387 absence of pegRNA targeting telomeres. 50.000 cells were seeded per well of µ-Slide 8 well
388 (Ibidi) chambered coverslip plates. Pre-extraction was performed using 0.1% Tween in PBS
389 24 hours after reverse transfection. Cells were then fixed with 4% para-formaldehyde and fixed
390 cells were processed for immunofluorescence using the following antibodies: anti-Cas9 (Cell
391 Signalling, 14697), anti-TRF1 (Abcam, ab1423), anti-MLH1 (ThermoFisher, A300-015A), anti-
392 MSH2 (Bethyl, A300-452A). Primary antibodies were diluted 1:500 and secondary antibodies
393 (Alexa Fluor® 568 goat anti-mouse and Alexa Fluor® 488 goat anti-rabbit, LifeTechnologies)
394 were diluted 1:2000.
395
396 **Imaging**
397 16-bit fluorescence images were acquired using an Olympus IXplore spinning disk confocal
398 microscope (equipped with the Yokogawa CSU-W1 with 50 µm pinhole disk and a Hamamatsu
399 ORCA Fusion CMOS camera). A 60X oil immersion objective (NA 1,42) in combination with a
400 3,2X magnification lens (equaling 192X total magnification) was used for superresolution
401 imaging of fixed cells and z-stacks with a 0,24µm slice interval were acquired. These z-stacks
402 were then processed using the Olympus 3D deconvolution software (constrained iterative
403 deconvolution, using automatic background removal and noise reduction, filter using
404 advanced maximum likelihood algorithm and 5 iterations). Finally "maximum-z" projection
405 images of the deconvoluted z-stacks were generated. For further data analysis, the ImageJ
406 (NIH) distribution FIJI was used. Nuclear foci were counted manually and at least 15 cells per
407 condition were imaged in each experiment. Quantification of the foci was performed manually
408 based on maximum intensity projections.
409
410
411 **References**
412 Acharya, S., Wilson, T., Gradia, T., Kane, M., Guerrette, S., Marsischky, G., et al. (1996).
413 hMSH2 forms specific mispair-binding complexes with hMSH3 and hMSH6. *Proc. Natl.*

Acad. Sci. U. S. A. 93, 13629–13634. doi:10.1073/PNAS.93.24.13629.

Anzalone, A. V, Randolph, P. B., Davis, J. R., Sousa, A. A., Koblan, L. W., Levy, J. M., et al. (2019). *Search-and-replace genome editing without double-strand breaks or donor DNA.* doi:10.1038/s41586-019-1711-4.

Bothmer, A., Phadke, T., Barrera, L. A., Margulies, C. M., Lee, C. S., Buquicchio, F., et al. (2017). Characterization of the interplay between DNA repair and CRISPR/Cas9-induced DNA lesions at an endogenous locus. *Nat. Commun.* 8, 13905. doi:10.1038/ncomms13905.

Brinkman, E. K., Chen, T., Amendola, M., and van Steensel, B. (2014). Easy quantitative assessment of genome editing by sequence trace decomposition. *Nucleic Acids Res.* 42, e168–e168. doi:10.1093/NAR/GKU936.

Cejka, P., Stojic, L., Mojas, N., Russell, A. M., Heinimann, K., Cannavó, E., et al. (2003). Methylation-induced G2/M arrest requires a full complement of the mismatch repair protein hMLH1. *EMBO J.* 22, 2245. doi:10.1093/EMBOJ/CDG216.

Charpentier, M., Khedher, A. H. Y., Menoret, S., Brion, A., Lamribet, K., Dardillac, E., et al. (2018). CtIP fusion to Cas9 enhances transgene integration by homology-dependent repair. *Nat. Commun.* 9, 1–11. doi:10.1038/s41467-018-03475-7.

Chen, B., Gilbert, L., Cimini, B., Schnitzbauer, J., Zhang, W., Li, G., et al. (2013). Dynamic imaging of genomic loci in living human cells by an optimized CRISPR/Cas system. *Cell* 155, 1479–1491. doi:10.1016/J.CELL.2013.12.001.

Clement, K., Rees, H., Canver, M. C., Gehrke, J. M., Farouni, R., Hsu, J. Y., et al. (2019). CRISPResso2 provides accurate and rapid genome editing sequence analysis. *Nat. Biotechnol. 2019 373* 37, 224–226. doi:10.1038/s41587-019-0032-3.

Drummond, J., Li, G., Longley, M., and Modrich, P. (1995). Isolation of an hMSH2-p160 heterodimer that restores DNA mismatch repair to tumor cells. *Science* 268, 1909–1912. doi:10.1126/SCIENCE.7604264.

Ferreira da Silva, J., Meyenberg, M., and Loizou, J. I. (2021). Tissue specificity of DNA repair: the CRISPR compass. *Trends Genet.* 0. doi:10.1016/J.TIG.2021.07.010.

Fishel, R. (2015). Mismatch repair. *J. Biol. Chem.* 290, 26395–26403. doi:10.1074/JBC.R115.660142.

Gaudelli, N. M., Komor, A. C., Rees, H. A., Packer, M. S., Badran, A. H., Bryson, D. I., et al. (2017). Programmable base editing of T to G C in genomic DNA without DNA cleavage. *Nature* 551, 464–471. doi:10.1038/nature24644.

Gradia, S., Acharya, S., and Fishel, R. (1997). The Human Mismatch Recognition Complex hMSH2-hMSH6 Functions as a Novel Molecular Switch. *Cell* 91, 995–1005. doi:10.1016/S0092-8674(00)80490-0.

Gu, S., Bodai, Z., Cowan, Q. T., and Komor, A. C. (2021). Base editors: Expanding the types

451 of DNA damage products harnessed for genome editing. *Gene Genome Ed.* 1, 100005.
452 doi:10.1016/J.GGEDIT.2021.100005.
453 Haugen, A. C., Goel, A., Yamada, K., Marra, G., Nguyen, T.-P., Nagasaka, T., et al. (2008).
454 Genetic Instability Caused by Loss of MutS Homologue 3 in Human Colorectal Cancer.
455 *Cancer Res.* 68, 8465–8472. doi:10.1158/0008-5472.CAN-08-0002.
456 Hussmann, J. A., Ling, J., Ravisankar, P., Yan, J., Cirincione, A., Xu, A., et al. (2021).
457 Mapping the Genetic Landscape of DNA Double-strand Break Repair. *bioRxiv*,
458 2021.06.14.448344. doi:10.1101/2021.06.14.448344.
459 Iyer, R., Pluciennik, A., Burdett, V., and Modrich, P. (2006). DNA mismatch repair: functions
460 and mechanisms. *Chem. Rev.* 106, 302–323. doi:10.1021/CR0404794.
461 Jinek, M., Chylinski, K., Fonfara, I., Hauer, M., Doudna, J. A., and Charpentier, E. (2012). A
462 programmable dual-RNA-guided DNA endonuclease in adaptive bacterial immunity.
463 *Science (80-.).* 337, 816–821. doi:10.1126/science.1225829.
464 Jiricny, J. (2006). The multifaceted mismatch-repair system. *Nat. Rev. Mol. Cell Biol. 2006*
465 *75* 7, 335–346. doi:10.1038/nrm1907.
466 Kadyrov, F., Dzantiev, L., Constantin, N., and Modrich, P. (2006). Endonucleolytic function of
467 MutLalpha in human mismatch repair. *Cell* 126, 297–308.
468 doi:10.1016/J.CELL.2006.05.039.
469 Koi, M., Umar, A., Chauhan, D. P., Cherian, S. P., Carethers, J. M., Kunkei, T. A., et al.
470 (1994). Human Chromosome 3 Corrects Mismatch Repair Deficiency and Microsatellite
471 Instability and Reduces N-Methyl-N′-nitro-N-nitrosoguanidine Tolerance in Colon Tumor
472 Cells with Homozygous hMLH1 Mutation. *Cancer Res.* 54.
473 Komor, A. C., Kim, Y. B., Packer, M. S., Zuris, J. A., and Liu, D. R. (2016). Programmable
474 editing of a target base in genomic DNA without double-stranded DNA cleavage.
475 *Nature* 533, 420–424. doi:10.1038/nature17946.
476 Li, G., and Modrich, P. (1995). Restoration of mismatch repair to nuclear extracts of H6
477 colorectal tumor cells by a heterodimer of human MutL homologs. *Proc. Natl. Acad. Sci.*
478 *U. S. A.* 92, 1950–1954. doi:10.1073/PNAS.92.6.1950.
479 Lipkin, S., Wang, V., Jacoby, R., Banerjee-Basu, S., Baxevanis, A., Lynch, H., et al. (2000).
480 MLH3: a DNA mismatch repair gene associated with mammalian microsatellite
481 instability. *Nat. Genet.* 24, 27–35. doi:10.1038/71643.
482 Palombo, F., Gallinari, P., Iaccarino, I., Lettieri, T., Hughes, M., D'Arrigo, A., et al. (1995).
483 GTBP, a 160-kilodalton protein essential for mismatch-binding activity in human cells.
484 *Science (80-.).* 268, 1912–1914. doi:10.1126/SCIENCE.7604265.
485 Palombo, F., Iaccarino, I., Nakajima, E., Ikejima, M., Shimada, T., and Jiricny, J. (1996).
486 hMutSβ, a heterodimer of hMSH2 and hMSH3, binds to insertion/deletion loops in DNA.
487 *Curr. Biol.* 6, 1181–1184. doi:10.1016/S0960-9822(02)70685-4.

Petri, K., Zhang, W., Ma, J., Schmidts, A., Lee, H., Horng, J. E., et al. (2021). CRISPR prime editing with ribonucleoprotein complexes in zebrafish and primary human cells. *Nat. Biotechnol. 2021*, 1–5. doi:10.1038/s41587-021-00901-y.

Pluciennik, A., Dzantiev, L., Iyer, R. R., Constantin, N., Kadyrov, F. A., and Modrich, P. (2010). PCNA function in the activation and strand direction of MutLα endonuclease in mismatch repair. *Proc. Natl. Acad. Sci.* 107, 16066–16071. doi:10.1073/PNAS.1010662107.

Rees, H. A., Yeh, W.-H., and Liu, D. R. (2019). Development of hRad51–Cas9 nickase fusions that mediate HDR without double-stranded breaks. *Nat. Commun. 2019 101* 10, 1–12. doi:10.1038/s41467-019-09983-4.

Richardson, C. D., Kazane, K. R., Feng, S. J., Zelin, E., Bray, N. L., Schäfer, A. J., et al. (2018). CRISPR–Cas9 genome editing in human cells occurs via the Fanconi anemia pathway. *Nat. Genet.* doi:10.1038/s41588-018-0174-0.

Stojic, L., Brun, R., and Jiricny, J. (2004). Mismatch repair and DNA damage signalling. *DNA Repair (Amst).* 3, 1091–1101. doi:10.1016/J.DNAREP.2004.06.006.

Umar, A., Koi, M., Risinger, J. I., Glaab, W. E., Tindall, K. R., Kolodner, R. D., et al. (1997). Correction of Hypermutability, N-Methyl-N′-nitro-N-nitrosoguanidine Resistance, and Defective DNA Mismatch Repair by Introducing Chromosome 2 into Human Tumor Cells with Mutations in MSH2 and MSH6. *Cancer Res.* 57.

Wang, X., Kam, Z., Carlton, P. M., Xu, L., Sedat, J. W., and Blackburn, E. H. (2008). Rapid telomere motions in live human cells analyzed by highly time-resolved microscopy. *Epigenetics Chromatin 2008 11* 1, 1–19. doi:10.1186/1756-8935-1-4.

Winter, G. E., Buckley, D. L., Paulk, J., Roberts, J. M., Souza, A., Dhe-Paganon, S., et al. (2015). Phthalimide conjugation as a strategy for in vivo target protein degradation. *Science (80-.).* 348, 1376–1381. doi:10.1126/SCIENCE.AAB1433.

Yeh, C. D., Richardson, C. D., and Corn, J. E. (2019). Advances in genome editing through control of DNA repair pathways. *Nat. Cell Biol.* 21(12), 1468–1478. doi:10.1038/s41556-019-0425-z.

Data availability

All sequencing data will be deposited in the European Nucleotide Archive (EMBL-EBI).

Competing Interests

The authors declare no commercial or financial relationships that could be construed as potential conflict of interest.

524

525 **Author Contributions**

526 JFdaS, GO, JJ and JIL conceptualized the study. JFdaS and JIL obtained funding. JFdaS,
527 GO, EA and AM carried out investigations. GT performed the confocal microscopy. JFdaS
528 performed analysis and visualization. JIL supervised the study. JFsaS with input from JIL
529 wrote the original draft and all authors reviewed and edited the final manuscript.

530

531 **Funding**

532 JFdaS is supported by a DOC fellowship from the Austrian Academy of Sciences
533 (ÖAW25035). A.M. is funded by the Austrian Science Fund, grant number P 33024 awarded
534 to J.I.L. The Loizou lab is funded by an ERC Synergy Grant (DDREAMM Grant agreement ID:
535 855741). CeMM is funded by the Austrian Academy of Sciences.

536

537 **Acknowledgments**

538 We would like to thank the VBCF (Vienna, Austria) for all next generation sequencing. We
539 would like to acknowledge Dr Jacob Corn (ETHZ, Zurich, Switzerland) and Dr Richard
540 Sherwood (Harvard Medical School, Boston, USA) for critically reading the manuscript. We
541 would like to thank Mr Chris Fell (Medical University of Vienna, Vienna, Austria) and Mr Marc
542 Wiedner (CeMM, Vienna, Austria) for technical support. We are thankful to Prof KJ Patel
543 (Weatherall Institute of Molecular Medicine, Oxford, UK) for providing the FANCD2 deficient
544 HAP1 cell line. The Winter Lab (CeMM, Vienna, Austria) provided valuable tools for protein
545 degradation. We are grateful to members of the Loizou lab for helpful discussions and
546 feedback.